Effectiveness of FRCM Reinforcement Applied to Masonry Walls Subject to Axial Force and Out-Of-Plane Loads
Evaluated by Experimental and Numerical Studies

(Article begins on next page)

08 February 2025

Effectiveness of FRCM reinforcement applied to masonry walls subject to axial force and out-of-plane loads evaluated by experimental and numerical studies

Alessandro Bellini

CIRI Buildings & Construction, University of Bologna, Bologna, Italy

Via del Lazzaretto 15/5, 40131, Bologna, BO, Italy.

Tel: 051/2090553, email: alessandro.bellini5@unibo.it

Andrea Incerti

CIRI Buildings & Construction, University of Bologna, Bologna, Italy

Via del Lazzaretto 15/5, 40131, Bologna, BO, Italy.

Tel: 051/2090553, email: andrea.incerti3@unibo.it

Marco Bovo

DICAM, University of Bologna, Bologna, Italy

Viale Risorgimento 2, 40136, Bologna, BO, Italy.

Tel: 051/2093246, email: marco.bovo@unibo.it

Claudio Mazzotti

DICAM, University of Bologna, Bologna, Italy

Viale Risorgimento 2, 40136, Bologna, BO, Italy.

Tel: 051/2093251, email: claudio.mazzotti@unibo.it

An experimental campaign and a numerical analysis devoted to the investigation of the out-of-plane behaviour of masonry walls reinforced with Fiber Reinforced Cementitious Matrix (FRCM) are presented here. The main goal of this study is to analyze and evaluate the effectiveness of the strengthening system, by discussing failure modes and capacity of strengthened masonry walls, in order to assess their behaviour under out-of-plane horizontal actions, such as, for example, seismic actions. A purposely designed experimental set-up, able to separately and independently apply an axial force and out-of-plane horizontal actions on masonry walls, was used. Experimental results are discussed and compared with the outcomes of nonlinear analyses performed on simplified finite element models of the walls. A proper evaluation of the flexural capacity of FRCM strengthened walls is the first step of the ongoing process of drawing reliable code guidelines leading to a safe design of strengthened masonry structures.

Keywords: FRCM, masonry wall, strengthening interventions, out-of-plane behaviour, Digital Image Correlation, FE model

Introduction

The growing awareness of the seismic vulnerability of our cultural heritage is leading to a much more careful design of necessary strengthening interventions. In order to better preserve the original architectural insight and to comply with the complex mechanical behaviour of masonry buildings, structural strengthening with composite materials is one of the most recent and effective techniques. This type of retrofitting system is becoming more and more common, in

particular when the aim is to strengthen the structure without increasing too much its weight and stiffness and changing its design philosophy. In this framework, it should be noted as the use of Fiber Reinforced Cementitious Matrix (FRCM) composite materials provides several advantages if compared to traditional strengthening techniques. In particular, these materials are often preferable to Fiber Reinforced Polymers (FRP), due to some important aspects, such as applicability on wet surfaces, permeability, fire resistance and removability. Several studies have been carried out regarding masonry specimens strengthened by FRP (Carloni et al., 2012, Carrara et al., 2013, de Felice et al., 2015, Kwiecień et al., 2015, Mazzotti et al., 2015a, b, c, Sassoni et al., 2017), but only few studies can be found concerning masonry walls strengthened with FRCM composite materials (Ferretti et al., 2016), especially for what concerns their out-of-plane behaviour.

Most of the previous experimental studies on masonry walls reinforced with mortar-based composites consist of three-point or four-point bending tests carried out on medium-scale samples, in which specimens, placed horizontally (Papanicolau et al., 2008, Harajli at al., 2010, Papanicolau et al., 2011, Valluzzi et al., 2014), were subjected to monotonic or cyclic loading until failure. In some cases, with no compression applied perpendicular to the mortar joints, no reliable data on unreinforced samples are available. Other studies were carried out on full-scale specimens placed in vertical position and subjected to a uniform out-of-plane pressure, applied my means of an air bag (Babaeidarabad et al., 2014). In another case, a full-scale U-shaped wall assembly composed of a façade and two transverse walls was subjected to a series of natural accelerograms by using a shaking table (De Santis et al., 2016).

3

In this framework, the aim of the ongoing research is to improve the understanding of failure mechanisms occurring when FRCM-strengthened masonry walls are subject to out-of-plane actions and constant axial load. To this purpose, an experimental set-up was developed, allowing to apply axial force and out-of-plane horizontal actions on a full-scale masonry wall separately and independently, with the wall placed in vertical position. A combined system of horizontal forces allowed to simulate the effect of a uniform distributed load applied along the height of the sample.

The objectives of the work were the analysis of the bond behaviour between the layer of reinforcement and the substrate, in order to evaluate the possible different failure modes, the investigation of mechanical performances of different commercially available common types of reinforcement systems obtained from full-scale structural elements and the comparison with results coming from more conventional bond tests. A uniform axial stress equal to 0.2 MPa was chosen, in order to simulate the typical axial stress distribution acting on masonry panels of rural building of Southern Europe. Higher levels of axial stress (which will be investigated in the future) are expected to produce a more brittle failure due to the energy releasing but with similar characteristic (fibers failure). In the present paper, preliminary results of this more extended experimental campaign are reported. In particular, the purposely designed experimental set-up will be described and the results from the tested walls will be analyzed in terms of failure type, maximum load, displacements, strain distributions and 3D strain maps obtained by Digital Image Correlation (DIC) technique.

Two different reinforcement layouts were tested: the first one characterized by bi-directional glass grids applied on the whole surface of the masonry wall, in combination with lime-based mortars, with or without the addition of an adhesion promoter and the second one realized by using steel fibers and a lime-based mortar, following a discontinuous layout. After the description of the experimental results, a first comparison with simple theoretical models will be presented, by discussing how to take into account the contribution of the FRCM strengthening system into a design approach, in relation to the identified failure mode and specifying that a guideline for evaluating the capacity of masonry elements strengthened with FRCM does not exist yet.

The study of the strengthened walls was pursued also by non-linear numerical analyses, performed on detailed finite element models of the wall-reinforcement system. The main outcomes of the numerical analyses, carried out for both continuous and discontinuous reinforcements, will be discussed for a better understanding of the real mechanisms governing the failure of the walls.

Experimental campaign

Experimental program and samples preparation

In order to evaluate the out-of-plane behaviour of masonry walls strengthened by FRCM composites, several full-scale samples of double-leaf masonry walls with dimensions $1.20\times0.25\times2.70$ m^3 were prepared. They were built by a professional mason, in order to avoid

differences in hand work and mortar workability among different specimens. Since the purpose was to investigate the mechanical behaviour of ancient historical masonry, wall specimens were realized by using medium-low strength clay bricks and low strength hydraulic lime mortar.

After a proper curing period of the walls of about two months under laboratory conditions, they were pre-loaded with a vertical stress of about 0.20 MPa, applied by tensioning four M20 steel bars (connected to two rigid steel plates placed respectively at the top and at the bottom of the walls), making use of a torque wrench previously calibrated by means of a load cell and monitoring this phase with strain gauges applied on the bars. The application of a distributed axial load was used here to simulate the stress state of a real masonry wall already present before the application of the strengthening system.

The different reinforcement layouts used for the strengthening of masonry walls are described in Table 1: in particular, GFRCM_01 and GFRCM_02 masonry samples were reinforced with bidirectional glass grids embedded in lime-based mortars following a continuous layout (Figure 1b,c), whereas SRG_01 is characterized by the application of a discontinuous reinforcement realized by three 100 mm wide unidirectional steel sheets embedded in a lime-based mortar (Figure 1d).

It should be noted that the reinforcement was placed only on the side that would be subject to traction during the out-of-plane test, since here the main interest lays on the mechanical behaviour of FRCM under traction. Furthermore, the potential resisting contribution in compression of the mortar matrix when placed on the compression side of the sample, consisting in a slight increase of the depth of the section, can be neglected here, considering the

6

reduced total thickness (between 6 and 8 mm) of the applied FRCM reinforcement.

The application of the strengthening system followed a standard procedure (Figure 2): application of the first mortar layer (about 3 mm thick) on the surface of the masonry wall, embedment of the composite reinforcement and finishing with a second layer of mortar (about 3 mm). Only for GFRCM_01 sample, the grid was impregnated with an adhesion promoter. During the reinforcement application, masons had also paid attention to not attach the FRCM composite on the whole masonry surface, adopting an offset of about 2 cm from top and bottom edges, in order to prevent buckling behaviour of reinforcement layer that could trigger early debonding phenomena during the pre-loading compression phase (Incerti et al., 2015). However, the adoption of the previously described tensioned steel bars, still present during reinforcement application and the choice of a constant axial stress of 0.2 MPa during the test (the same applied through the steel bars), allowed to avoid the transmission of potential compressive stresses to the FRCM reinforcement. The application of the composite reinforcement by using a predefined offset from left and right edges of the wall allowed also to analyze the behaviour of the small portions of unreinforced masonry and to locate strain and cracks in relation with masonry texture (bricks or mortar joints) by using DIC technique.

Materials characterization

All the materials used for the realization of masonry walls and FRCM strengthening systems were carefully characterized from a mechanical point of view. The adopted new clay bricks used for construction of masonry panels were characterized in terms of compressive, flexural and splitting tensile strength. For assessing compressive strength in the direction perpendicular and

parallel to the bed face (according to Mazzotti et al., 2015c), cylindrical samples with 50 mm diameter and 50 mm height were cored from bricks and then tested under compression loading (Figure 3a). Similar cores were also used for assessing the tensile splitting strength by means of indirect tensile tests. Finally, flexural strength was obtained by testing prismatic portions of brick under three-point bending scheme, according to EN 12372:2006. Results in terms of mean compressive (f_{bc}), flexural ($f_{bt,flex}$) and splitting ($f_{bt,split}$) tensile strength are reported in Table 2. It should be noted that a proper characterization of bricks is required for an accurate description of masonry wall properties and for determining the correct parameters needed as input for the FE models.

Mechanical characterization of natural hydraulic lime (NHL) based mortars used for mortar joints preparation and for the application of FRCM strengthening systems was carried out by means of standard three-point bending tests on mortar prisms ($40 \times 40 \times 160$ mm^3) and compressive tests on the two remaining broken parts, according to UNI EN 1015-11:2007 (see Figure 3b). Mean compressive strength (f_{mc}) and flexural tensile strength (f_{mt}) of mortars are reported in Table 3. As can be observed from Table 3, the mortar used to produce the walls had very low strength, typical of existing masonry, while those used for strengthening systems application are modern performing mortars.

In order to evaluate the behaviour of reinforced masonry walls subjected to out-of-plane forces for different layouts, three different types of strengthening systems were tested in the experimental campaign:

8

1)   A balanced bidirectional glass grid (Type 1 in Figure 1b), one meter wide, was used for GFRCM_01 sample, with a density of 300 g/m^2 and a nominal bundle spacing of 12 mm. The equivalent dry fiber thickness of the applied grid was 0.06 mm. Maximum tensile strength and elastic modulus specified by the producer for the use of the grid in FRCM composites, are, respectively, 1000 MPa and 65 GPa. Previous experimental tensile tests performed on these GFRCM composites showed a mean value of 1165 MPa for the ultimate tensile strength of the fiber (Bellini et al., 2016). As common application from the producer, in this type of reinforcement system an adhesion promoter was used, characterized by a flexural strength of 5 MPa, by an elastic modulus of 4.5 GPa and by an ultimate deformation of 1.2% (producer data). The total thickness of the applied GFRCM strengthening system (composed by a mortar layer, a single layer of GFRCM reinforcement grid and then another mortar layer) was about 6 mm.

2)   A different type of balanced bidirectional glass grid (Type 2 in Figure 1c) was used for GFRCM_02 specimen, characterized by a density of 300 g/m^2, a nominal bundle spacing of 18 mm and an equivalent thickness of 0.055 mm. Maximum tensile strength and elastic modulus are, respectively, 1050 MPa and 70 GPa (producer data). Previous experimental tensile tests showed a mean value of 790 MPa for the ultimate tensile strength of the composite. The total thickness of the reinforcement system was about 6 mm.

3)   A unidirectional sheet made of ultra-high strength galvanized steel micro-cords (Type 3 in Figure 1d), 100 mm wide, was used for SRG_01 sample. It was characterized by a density of 600 g/m^2, an equivalent thickness of 0.084 mm and by the presence of 16 cords within the width of the band. Maximum tensile strength and elastic modulus specified by the producer are,

respectively, 3000 MPa and 156 GPa. The total thickness of the applied steel strengthening system (composed by a mortar layer, a single layer of steel reinforcement and then another mortar layer) was about 8 mm.

Test set-up

A specific vertical set-up was used for the out-of-plane tests (see Figure 4), able to apply distributed horizontal forces to the wall along its out-of-plane direction, together with a constant longitudinal axial stress distribution, corresponding to the presence of overhanging loads from upper storeys. The wall, placed in vertical position, is double hinged at its extremities (top and bottom) and it is kept in position by a horizontal restraining system, composed of two steel trusses connected to the reaction wall at the top and of steel connections to the strong floor at the bottom. Four horizontal forces were applied along the height of the wall by means of two double-hinged steel systems transmitting forces produced by two hydraulic jacks with a maximum capacity of 150 kN, allowing to obtain a bending moment distribution quite similar to that produced by a uniform distributed load.

Finally, in order to keep constant the vertical axial stress (where $\sigma = 0.2$ MPa) during the test, two hydraulic jacks were positioned at the top of the upper hinge and connected to the strong floor by using two Dywidag rods. The chosen axial stress was maintained during the set-up preparation by gradually applying axial stress through the hydraulic jacks while the tensioned steel bars, originally used to maintain the vertical stress during the application and the curing phase of the FRCM reinforcement, were carefully loosened and monitoring the displacement of the upper steel plate. Horizontal and vertical forces were applied to the sample by using two

10

independent hydraulic systems, with two separate circuits and dedicated hydraulic pumps.

The horizontal forces were applied monotonically well beyond the appearance of non-linear degradation, after which an unloading and reloading cycle was performed reaching the final failure.

Instrumentations

In order to analyze out-of-plane displacements related to bending and shear phenomena, different types of instruments were used. In particular, horizontal displacements at the wall extremities (top and bottom) and at mid-height were measured by displacement transducers (LVDTs) or draw-wire displacement transducers (WDTs). Two further LVDTs were used to measure relative rotations of the bottom hinge.

All the applied forces were measured by using pressure transducers. In particular, any possible variation of the vertical load during the test was monitored by using a dedicated pressure transducer and the load was maintained constant by using its own hydraulic system.

The side of the specimen under traction was prepared for the application of Digital Image Correlation (DIC) technique, by creating a random speckle pattern by means of a white paint and black dots, realized by using appropriate size markers. It should be noted that the choice of a suitable speckle pattern at this stage is very important to reach the required accuracy during the post-processing phase. The size of black dots was chosen in order to maximize accuracy without generating additional noise on the acquired images: small speckles of about 3-5 pixels in size (between 2.0 and 3.3 mm in real dimensions, in this case) proved to be the best choice. A stereoscopic system based on two high resolution (5 MP) digital cameras with a focal length of

23 mm, positioned with a baseline of 900 mm and with an angle of about 15 degrees between them, was used to monitor 3D full-field surface displacements and deformations of the sample, reaching a pixel size (in real dimensions) of about 0.65 mm. A f-number (defined as the ratio of the lens focal length to the diameter of the entrance pupil) of 5.6 was chosen during image acquisition. Further details on the application of this innovative full-field optical method can be found in Mazzotti et al. (2015b). The application of DIC technique allowed obtaining the complete 3D displacement and strain maps of the front side of the tested specimens and not only in pre-assigned points.

Finally, only for GFRCM_01 specimen, vertical deformations of the FRCM surface along its centerline were measured by using seven strain gauges properly spaced (with 80 mm of spacing). This choice allowed analyzing and comparing strain data coming from different measurement techniques.

Experimental Results and Discussion

Experimental results

All the tests were characterized by a vertical stress $_{.}$ = 0.20 MPa, imposed to the wall at the beginning and kept constant throughout it. The horizontal forces were applied monotonically well beyond the end of the first almost linear phase and the appearance of non-linear degradation (usually fibers slippage), after which, through the load cycle, the effect of fibers slippage on stiffness degradation was observed.

Figure-5 shows the typical flexural failure modes observed from the three tests carried out. All the tests were concluded by the tensile failure of the reinforcement in the central portion of the sample, where the bending moment was constant and maximum. In detail, failure occurred exactly at mid-height of the specimen (SRG_01) or just below (GFRCM_01) or above (GFRCM_02) the mid-height level. As expected, the critical cross-section (i.e. the section where final failure occurred) was always located at the level of a mortar joint, which was cracked. In particular, Figure 6 shows that failure of GFRCM_01 wall occurred within the reinforcement in correspondence of a crack previously opened at brick-mortar interface. The critical cross-section of GFRCM_02 and SRG_01 samples was located, instead, close to brick-mortar interface, but within the mortar layer.

Only in the case of discontinuous reinforcement (SRG_01), the failure of steel fibers was accompanied by the detachment of a triangular wedge of masonry (Figure 5c) due to the strong concentration of shear stresses occurring below the reinforcing strips.

Maximum bending moment-deflection curves of the reinforced masonry walls are reported in Figure 7. GFRCM_01 sample (see Figure 7a) showed a first almost linear-elastic branch up to the onset of cracking phenomena, clearly identifiable in the graph (Point A) by the sudden change in slope. It should be noted that different load cycles were performed during the test in order to evaluate residual deformations with increasing level of horizontal applied force; the first cycle performed along the initial branch (5 kNm) confirmed the almost linear-elastic behaviour of the sample at this stage.

Cracking, as expected, occurred along the mortar joints spreading from the central part of the wall towards the extremities. Cycles inside the cracked phase showed a reducing secant

13

stiffness corresponding to a progressive damaging of the system. Cracks opening and spreading along the height of the wall provided for the characteristic non-linear behaviour of the monotonic envelope leading to the final failure. The maximum registered bending moment was 22.38 kNm, whereas a maximum deflection of 51.92 mm was measured just before failure.

GFRCM_02 specimen showed a bilinear behaviour, with a first almost linear branch up to Point A (see Figure 7b) and a second branch with a reduced stiffness that led to the final failure (Point D), corresponding to a maximum bending moment of 18.97 kNm and to a deflection of 29.26 mm. As for GFRCM_01 specimen, the first cycle performed along the initial branch confirmed the almost linear-elastic behaviour of the sample during this phase, without inelastic or residual deformation.

SRG_01 sample (Figure 7c) revealed a different behaviour: it is characterized by two main branches with a continuous transition between them. In comparison with the other specimens, it showed a higher slope of the second branch. Even if the overall stiffness of the different reinforcements was similar ($EA \cong 3900$ kN smeared over 1000 mm width), the local stiffness of the SRG was much higher ($EA_L \cong 1310$ kN smeared over 100 mm width); as a consequence, the effectiveness of the bond behaviour was higher, producing smaller slips inside the mortar and increasing the slope of the curve. Failure occurred at a maximum bending moment of 30.07 kNm, in correspondence of a deflection of 67.49 mm (Point C). In all cases, the strong deformability of the specimens after the knee point is due to slippage of the fibers inside the mortar layer; in fact, glass fibers are elastic until failure and they cannot provide for the observed equivalent "*plastic*" behaviour.

14

Figure-8 shows the out-of-plane deflection of GFRCM_01 wall, recorded with DIC technique for increasing values of the applied forces. If at the beginning of the test the wall is quite uniformly bended, close to failure the curvature demand is mainly concentrated in the central portion of the wall, due to the non-linear effect of cracking. Nevertheless, the presence of FRCM reinforcement prevents the formation of one single "plastic hinge" at mid-height, which would lead to sudden failure; on the contrary, a wide portion of the wall was cracked but still able to carry the external loads. This type of deformation pattern allows for obtaining large out-of-plane capacity and it increases the corresponding ductility.

Strain maps provided by DIC technique at increasing load levels applied on GFRCM_01 sample are reported in Figure 9; they clarify, if necessary, that cracks started from mortar joints and they caused evident localized variations in the strain field (red thin lines). In correspondence of the strengthened part of the wall, nevertheless, FRCM allowed a certain level of redistribution of deformation (smoother variation of colours) due to the tensile capacity of the composite grid. This can be observed by zooming on the lateral sides of the wall, where there is the transition between the plain masonry (10 cm from the lateral side of the wall) and the strengthened part; in those positions, the thin red lines across the joints become wider and less intense (colour change) over the reinforcement, peaks interesting here also the bricks. Variations in the strain field caused by matrix cracking were already detected in other studies (Bellini et al., 2015) during several bond tests performed on CFRCM and GFRCM composite applications on masonry samples. In this case, though, the presence of out-of-plane bending imposed an increasing curvature to the substrate, triggering and localizing the cracks in the weakest cross-sections (mortar joints) and imposing a predefined crack spacing. This is not exactly what usually

happens during bond tests, where the curvature effect is not present and it is one of the reasons why results can be different, leading also to different failure modes.

Figure-10 shows strain field evolution recorded on the surface of SRG_01 specimen: as for GFRCM_01 sample, cracks started clearly in correspondence of the mortar joints and the presence of a discontinuous reinforcement layout allowed the observation of evident strain redistribution, with a significant reduction of the strain peaks. This particular behaviour can be observed in detail in Figure 11, where a comparison between strain profiles measured by using DIC technique on the plain masonry wall surface and on the adjacent strengthened wall surface, along two different lines of recording, is presented. Peaks of different amplitude can be observed: the lower the strain peak, the larger its diffusion over the wall surface.

Another example of strain maps, concerning GFRCM_02 sample, is reported in Figure 12. The cracking pattern confirms that, as for the other walls, cracks started from mortar joints, but, in this case, the behaviour is not so regular, with a more reduced strain redistribution: the different strengthening system used (mortar and fibers) allows for a different bond capacity; as a consequence, larger slips took place with a stronger localization. Nevertheless, also in this case the fibers failure was attained, since the available bond length was very long (meters from mid-height) and when local debonding started, bond forces were transmitted to the cross-sections less stressed (in proximity of the extremities).

Finally, a comparison between strain gauges readings along the specimen centerline and strain profiles obtained by the application of DIC technique is presented in Figure 13 for specimen GFRCM_01; in the same figure, the positions of strain gauges with respect to the brick

and mortar joint texture are also reported. An acceptable correlation can be found between the two strain distributions corresponding to points B and C of Figure 7a, where the cracking patterns were still quite limited. When considering conditions close to the final failure of the wall (point G), the strain distributions become remarkably different. Larger variations can be found in correspondence of strain gauges placed over the mortar joints or close to them. In that cases, cracks that are opening in correspondence of the mortar joints, can be captured by DIC technique only if an appropriate (quite small) subset (sub-image used for displacement tracking, defined in terms of number of pixels) and a correct step size (distance between data points) are chosen. On the contrary, they are more difficult to be identified by strain gauges that were probably reading a strain value not only in correspondence of the mortar joint, but averaged along the gage length (20 mm), so considering also adjacent portions of the brick. In this context, DIC results seem more accurate and reliable.

Comparison with theoretical models

Even if a specific guideline for evaluating the capacity of masonry elements strengthened with FRCM systems does not exist yet, available experimental tests showed that the maximum contribution of reinforcement is strongly dependent on the identified failure mode. In case of debonding or delamination within the mortar layer, FRCM contribution could be estimated by using some predictive formulas contained inside the Italian Guidelines for the design and construction of externally bonded FRP systems (CNR, 2013). Indeed, a comparison between the maximum bending moment registered during the tests and the theoretical one calculated by using design formulas suggested by Italian guidelines is presented in the following. In particular,

17

FRCM mechanical performances can be obtained by extending the validity of the FRP analytical formulation to the actual strengthening system. Making use of the fracture energy concept, the theoretical debonding force of GFRCM composite could be written as:

$$F_{max,th,db} = b_f \sqrt{2E_f t_f k_b k_G \sqrt{f_{bc} f_{bt}}}, \tag{1}$$

where f_{bc} and f_{bt} are mean brick compressive and tensile strength, k_b and k_G are corrective coefficients, E_f, t_f and b_f are, respectively, elastic modulus, thickness and width of the reinforcement. But in case of FRCM, the failure mode is delamination within the mortar layer instead of cohesive debonding inside the substrate; for this reason, a useful modification of Equation (1) is that of using mortar mechanical properties rather than brick compressive and tensile strength. Equation (1) can be then modified in the following form:

$$F_{max,th,del} = b_f \sqrt{2E_f t_f k_b k_G \sqrt{f_{mc} f_{mt}}} \tag{2}$$

where f_{mc} and f_{mt} are, respectively, mean mortar compressive and tensile strength, as already discussed during materials characterization. It should be noted that these analytical formulations could be directly compared with results coming from more conventional bond tests in order to assess their validity and to calibrate corrective coefficients. However, since calibration of Equation (2) is not the purpose of this paper, results coming from this modified predictive formulation will be used only for comparison with experimental outcomes, adopting values of corrective coefficients contained inside CNR Italian Guidelines, in order to check if a satisfactory prediction can be obtained.

On the contrary, if the system failure is due to fibers tensile rupture, the maximum tensile force that can be transferred by the reinforcement to the substrate is defined starting from the tensile strength of the FRCM strengthening system. As an example, for the GFRCM_01 sample, preliminary tensile tests on specific coupons showed a mean tensile strength of 1165 MPa; similarly, bond tests on the same system revealed that tensile failure of fibers outside of the bonded area was the most common failure mode, but with a mean strength value of 801 MPa, referred to the dry fibers cross-section (Bellini et al., 2016). This smaller stress value is due to the limited capacity of the unbonded grid to redistribute tensile forces across the bundles thus leading to stresses localization, happening at the interface between the bonded and the unbonded part. Starting from the identified materials properties coming from tensile and bond tests performed on GFRCM_01 strengthening system, a simple evaluation of the flexural capacity of the masonry wall under combined axial load and bending moment was performed, as suggested by Italian code (NTC 2008), by using the hypothesis of plane sections. As a result, the predicted maximum bending moment was 22.80 kNm in case of debonding, 21.84 kNm in case of delamination inside the mortar layer and finally 23.31 kNm if fiber rupture is reached. If the strength value determined during single-lap shear tests was considered in the calculation, a maximum bending moment of 18.50 kNm could be estimated.

Extending this approach to GFRCM_02 sample also, the following maximum bending moments can be estimated: 22.50 kNm in case of debonding, 21.76 kNm in case of delamination and finally 18.49 kNm if tensile rupture of the fibers occurs. If results coming from conventional bond tests are considered (with a mean strenght value of 623 MPa), a maximum bending moment of only 16.10 kNm can be expected.

Finally, considering the maximum tensile strength of the steel fibers sheets applied on SRG_01 sample, a maximum bending moment of 25.79 kNm could be estimated for this reinforcement system.

Results of the evaluation of the flexural capacity of the strengthened walls, in relation to the different failure modes, are summarized in Table 4, where, for comparison purposes, the estimated maximum bending moment of an unreinforced masonry (URM) wall is also reported. The capacity of the URM wall was evaluated by means of a simplified model assuming a collapse mechanism due to the formation of three plastic hinges with the splitting of the wall into two rigid blocks (Augusti et al., 2001).

Comparison with experimental results shows that by using bond strength coming from bond tests an underestimation of the maximum capacity of reinforced masonry walls subjected to out-of-plane forces can be obtained and that, in real applications, longitudinal stresses inside the reinforcement at failure are very similar to its tensile strength, exploiting its full capacity. As introduced before, this is because of the capacity of the strengthening system to increase the applicable force even after the local debonding, since the effective bonded part has been shifted in a less stressed portion of the wall.

Numerical analysis for the interpretation of experimental tests

Description of the finite element model

In order to better understand the structural behaviour of the strengthened walls under out-of-plane forces, a nonlinear finite element (FE) model was adopted, obtained starting from the

20

geometry of the real specimens. Due to the particular restraint and loading conditions imposed during the tests (i.e. cylindrical hinge assumption at the top and at the base and several concentrated loads distributed along the transversal direction), it is reliable to introduce the hypothesis of plane stress condition for the vertical sections of the walls. Therefore, a plane FE model was considered for the study of the out-of-plane behaviour of the tested walls GFRCM_01 and SRG_01 (see Figure 14), with the only differences related to the different geometrical and mechanical properties of the reinforcement. A refined mesh was adopted to describe the geometry, modelling in detail bricks, horizontal and vertical lime mortar joints constituting the original walls, the two layers of lime based mortar of the strengthening system and the composite grid embedded in it (considered as a uniform layer). The mesh is constituted by isoparametric four nodes finite elements and, in order to introduce the bond-slip behaviour between the reinforcement grid and the two layers of mortar in which the grid is embedded, interface elements were adopted at those surfaces.

The restraining system is achieved by means of a hinge located at the bottom of the wall and a vertical roller at the top allowing the application of the vertical load. Coherently with the experimental campaign, the loads in the model were applied in two phases: in the first one the vertical load only was applied and then maintained constant during the second phase of loading, in which the horizontal forces were assigned. Each horizontal force was applied to a surface equal to the real contact length adopted in the test, so as to spread to the masonry wall the concentrated load of the hydraulic jacks (see Figure 14). The numerical analyses were performed with DIANA package (DIANA 2016) considering static loading conditions.

21

The mechanical properties and the more suitable constitutive laws for the different materials were defined starting from the outcomes of the preliminary mechanical characterization tests. In order to capture in a realistic way the nonlinear behaviour of the specimens, different inelastic constitutive laws for the different materials were adopted. A smeared total strain crack model (Rots et al., 1985) was considered for the simulation of damage in the mortar (for both original wall and reinforcement layers). In the numerical models, the equivalent length h governing the fracture process was calibrated for the various elements following the indication furnished in Rots (1988). In this framework, damage both in tension and in compression was considered, by using a post peak exponential decay in tension and an elastic-plastic stress-strain relation under compression. With regards to fracture energy G_f, governing the tensile behaviour of mortar, a value of 0.12 N/mm was adopted and an equivalent length h of 2.8 mm was obtained following the considerations in Rots (1988). The strengths (both in compression and tension) obtained with the experimental tests and adopted for the two different types of mortar are reported in Table 3. From an accurate survey of the walls after the tests, brick elements appeared to be undamaged since degradation concentrated into mortar joints. For this reason, an elastic behaviour was adopted for the bricks and having a value of E = 4000 MPa. For the glass grid of GFRCM_01 specimen embedded in the reinforcement layer (which during the horizontal loading was subject to tensile forces) an elastic-brittle behaviour was adopted with an elastic modulus E = 69000 MPa and a tensile strength of 1165 MPa. Also the steel fiber sheets applied on SRG_01 specimen were considered as elastic-brittle with an elastic modulus E = 205000 MPa and a tensile strength of 3000 MPa.

The hysteretic behaviour of the mortar for cyclic loading is characterized by a secant unloading, pointing to the origin, and elastic reloading aiming to the unloading point in the stress-strain curve.

Finally, the bond-slip (τ-s) relation adopted for the interface elements between mortar and reinforcement grids was assumed bilinear with a first elastic branch followed by a softening linear response after the peak value. From the preliminary studies on mechanical characterization of the materials (Bellini et al., 2016), it was possible to roughly calibrate the values required to define the τ-s relation. Unloading and reloading of interface elements follow the elastic stiffness. The elastic unloading/reloading curve is followed until the inverse maximum traction value is reached, and from there the bond-slip curve is followed from the point where the bond-slip curve was left, in the opposite direction. In case the reloading is initiated from a point of the elastic unloading curve, the bond-slip curve is recaptured at the point where it was left (see DIANA 2016). The bilinear backbone curve was numerical defined by a peak value $\tau_{peak} = 0.2$ MPa; $s_{peak} = 0.06$ mm and an ultimate slip value equal to $s_{ultimate} = 0.25$ mm, providing for a constitutive bond-slip relation characterized by a fracture energy $G_f = 0.025$ N/mm, dissipated during delamination. This complex topic, concerning the evaluation of the nonlinear behaviour of mortar-reinforcement interface and the assessment of the anchorage length of the FRCM reinforcement to the substrate, will be object of future in-depth analysis. Moreover, the definition of a more suitable proposal for this type of local mechanism is not a goal of the present paper.

23

Numerical results and comparison with experimental outcomes

The numerical models previously described were used to reproduce the experimental tests performed on GFRCM_01 and SRG_01 specimens. As far as the comparison between experimental and numerical results is concerned, in Figure 7a the global curve of the horizontal wall deflection measured at the mid-height level of the wall *vs.* the bending moment applied at the same cross-section is reported. The monotonic envelope is properly captured, even during the evolution of the cracking pattern with consequent stiffness degradation. The unloading-reloading cycles located along the second branch of the envelope (points D-G), are roughly described by the model in terms of secant stiffness but poorly matched in terms of energy dissipation: this is due to the really simplified cyclic rules introduced in the model. The failure point in terms of horizontal deflection and ultimate bending moment is captured with excellent approximation. With regard to the structural behaviour of SRG_01 specimen (see Figure 7c), similar consideration can be drawn. The deformed shape of the wall along its height, for increasing values of applied horizontal forces, is shown in Figure 8 for GFRCM_01 sample. The numerical outcomes are in good agreement with the experimental results, both at the beginning of the test and near failure, where important debonding phenomena took place. The overall matching of the numerical results with experimental findings confirm that activation of debonding phenomenon increases the overall deformability of the system without leading immediately to failure. This is quite different from what can be observed from bond tests on relatively small specimens, particularly because in real cases shear forces are introduced in the reinforcement also by means of substrate curvature increment and not only by applying direct tensile forces.

As already discussed in the previous section, from a detailed survey after the test of GFRCM_01 specimen, a diffused cracking pattern emerged, with cracks that appear in the mortar joints for a considerable portion of the height of the wall and with cracks depth exceeding, at mid-height level, one half of the thickness of the wall. These aspects can also be found in the numerical results (see Figure 15), where the cracks are widespread for almost the whole height of the wall and a depth at the mid-height of more than one leaf of the wall.

Figure-16 shows the evolution of the strain distribution along the height of the wall, as obtained from the numerical analysis on the model of GFRCM_01 specimen for the load levels identified in Figure 7a (Point C, E and G). The mid-height portion of the wall is only considered in the graph and the strain distribution along four horizontal mortar joints and along the adjacent bricks is analysed. As expected, strain localized into the mortar joints, while the deformation on the adjacent bricks is much smaller (also more than four times in some cases). The bell shape distribution of strain corresponding to the joints often leaks over the bricks due to the smeared crack approach. Nevertheless, if the peak strain obtained numerically are compared with values emerged from the experimental tests (see strain contour of Figure 9) the ranges of the peaks are of the same order of magnitude. This as a further confirmation of the good matching between the real structural behaviour of the specimens detected during the out-of-plane tests and the outcomes of the numerical simulations.

Conclusions

In the present paper, the experimental behaviour of FRCM strengthening systems was

25

investigated with reference to the out-of-plane capacity of strengthened masonry walls. Full-scale tests were performed on vertical walls by using a specific experimental set-up, able to independently apply a longitudinal stress and out-of-plane horizontal forces. GFRCM and SRG strengthening systems were considered and the corresponding experimental outcomes were properly described. The reinforcement system proved to be effective, preventing the formation of the expected hinge at mid-height of the wall and redistributing forces over a large portion of it. In all cases, the identified failure mode was the tensile failure of the fibers, which occurred before the debonding of the reinforcement from the substrate. The application of Digital Image Correlation technique allowed to obtain a clear cracking pattern, strongly guided by the discontinuities represented by the wall mortar joints, that also triggered cracks inside FRCM matrix.

Structural tests showed that, when local debonding occurred, the system was capable of redistributing forces to portions of the wall with a lower bending moment, thus allowing for a further increment of displacement, if not of applied force, before the final failure.

Adoption of simple theoretical models and predictive formulas commonly used for FRP (Italian Guidelines) proved to be only partially effective, in particular because of the different failure mode. Introduction of some parameters modification improved the prediction capability but not satisfactorily due to the previous remark.

Experimental results have been discussed and compared with the outcomes of the nonlinear analyses performed on simplified finite element structural models of the walls, showing good agreement between experimental and numerical outcomes.

The aim of the presented research is to improve the knowledge about the out-of-plane behaviour of reinforced masonry walls and to investigate differences with more conventional bond tests, by considering also the role of mortar joints. In order to extend the experimental database, other tests on masonry walls characterized by continuous and discontinuous layouts are currently in progress, in parallel with other comparisons with analytical models and FE analyses.

Acknowledgements

References

Augusti G., Ciampoli M., Giovenale P. 2001. Seismic vulnerability of monumental buildings. Structural Safety 23:253-274.

Babaeidarabad S., De Caso F., and Nanni A. 2014. Out-of-plane behavior of URM walls strengthened with Fabric-Reinforced Cementitious Matrix Composite. Journal of Composites for Construction 18(4) DOI 10.1061/(ASCE)CC.1943-5614.0000457.

Bellini, A., Ferracuti, B., and Mazzotti, C. 2015. Effect of matrix on bond between FRCM and masonry. In *Proceedings of the 12th International Symposium on Fiber Reinforced Polymers for*

27

Reinforced Concrete Structures & The 5th Asia-Pacific Conference on Fiber Reinforced Polymers in Structures, Joint Conference. Nanjing, China, 14-16 December 2015.

Bellini, A., and Mazzotti, C. 2016. Bond behavior and tensile properties of FRCM composites applied on masonry panels. In *Proceedings of the 10th International Conference on Structural Analysis of Historical Constructions.* Leuven, Belgium, 13-15 September 2016.

Carloni, C., and Subramaniam, K.V. 2012. FRP-masonry debonding: numerical and experimental study of the role of mortar joints. Journal of Composites for Construction 16(5):581-589.

Carrara, P., Ferretti, D., and Freddi, F. 2013. Debonding behavior of ancient masonry elements strengthened with CFRP sheets. Composites Part B: Engineering 45(1):800-810.

CNR-DT 200 R1/2013. Guide for the Design and Construction of Externally Bonded FRP Systems for Strengthening Existing Structures. National Research Council, Rome.

de Felice, G., Aiello, M.A., Bellini, A., Ceroni, F., De Santis, S., Garbin, E., Leone, M., Lignola, G.P., Malena, M., Mazzotti, C., Panizza, M., and Valluzzi, M.R. 2015. Experimental characterization of composite-to-brick masonry shear bond. Materials and Structures 49:2581-2596. DOI 10.1617/s11527-015-0669-4.

De Santis, S., Casadei, P., De Canio, G., de Felice, G., Malena, M., Mongelli, M., and Roselli, I. 2016. Seismic performance of masonry walls retrofitted with steel reinforced grout. Earthquake Engineering and Structural Dynamics 45:229-251.

DIANA (2016). DIANA FEA User's Manual Release 10.1. Website: dianafea.com.

EN 12372. Natural stone test methods – Determination of flexural strength under concentrated load. 2006.

Ferretti, F., Incerti, A., Ferracuti, B., and Mazzotti, C. 2016. Diagonal compression tests on masonry panels strengthened by FRP and FRCM. In *Proceedings of the 10th International Conference on Structural Analysis of Historical Constructions.* Leuven, Belgium, 13-15 September 2016.

Harajli, M., ElKhatib, H., and Tomas San-Jose, J. 2010. Static and cyclic out-of-plane response of masonry walls strengthened using textile-mortar system. Journal of Materials in Civil Engineering 22(11):1171-1180.

Incerti, A., Vasiliu, A., Ferracuti, B., and Mazzotti, C. 2015. Uni-Axial compressive tests on masonry columns confined by FRP and FRCM. In *Proceedings of the 12th International Symposium on Fiber Reinforced Polymers for Reinforced Concrete Structures & The 5th Asia-Pacific Conference on Fiber Reinforced Polymers in Structures, Joint Conference.* Nanjing, China, 14-16 December 2015.

Iovinella, I., Prota, A., and Mazzotti, C. 2013. Influence of surface roughness on the bond of FRP laminates to concrete. Construction and Building Materials 40:533-542.

Kwiecień, A., de Felice, G., Oliveira, D.V., Zając, B., Bellini, A., De Santis, S., Ghiassi, B., Lignola, G.P., Lourenço, P.B., Mazzotti, C., and Prota, A. 2015. Repair of composite-to-masonry bond using flexible matrix. Materials and Structures 49: 2563-2580. DOI 10.1617/s11527-015-0668-5.

29

Mazzotti, C., Ferracuti, B., and Bellini, A. 2015a. Experimental Bond Tests on Masonry Panels Strengthened by FRP. Composites Part B: Engineering 80:223-237.

Mazzotti, C., Ferracuti, B., and Bellini, A. 2015b. Experimental study on masonry panels strengthened by GFRP: the role of inclination between mortar joints and GFRP sheets. Key Engineering Materials 624:559-566.

Mazzotti, C., Sassoni, E., Bellini, A., Ferracuti, B., and Franzoni, E. 2015c. Strengthening of masonry elements by FRP: Influence of brick mechanical and microstructural properties. Key Engineering Materials 624:330-337.

Mordanova, A., De Santis, S., and de Felice, G. 2016. State-of-the-art review of out-of-plane strengthening of masonry walls with mortar-based composites. In *Proceedings of the 10th International Conference on Structural Analysis of Historical Constructions.* Leuven, Belgium, 13-15 September 2016.

NTC 2008, D.M. 14 Gennaio 2008. Nuove Norme Tecniche per le costruzioni, Italian Ministry of Infrastructures and Transportation, Rome, 2008.

Papanicolaou, C.G., Triantafillou, T.C., Papathanasiou, M., and Karlos, K. 2008. Textile reinforced mortar (TRM) versus FRP as strengthening material of URM walls: out-of-plane cyclic loading. Materials and Structures 41:143-157.

Papanicolaou, C.G., Triantafillou, T.C., and Lekka, M. 2011. Externally bonded grids as strengthening and seismic retrofitting materials of masonry panels. Construction and Building Materials 25:504-515.

Rots, J.G., Nauta, P., Kusters, G.M.A. and Blaauwendraad, J. 1985. Smeared crack approach and fracture localization in concrete. Heron 30(1):3-48.

Rots, J.G. 1988. Computational modeling of concrete fracture. Dissertation, Delft University of Technology, Delft, Netherlands.

Sassoni, E., Andreotti, S., Bellini, A., Mazzanti, B., Bignozzi, M.C., Mazzotti, C., and Franzoni, E. 2017. Influence of mechanical properties, anisotropy, surface roughness and porosity of brick on FRP debonding force. Composites Part B: Engineering 108:257-269.

UNI EN 1015-11. Methods of test for mortar for masonry – Part 11: Determination of flexural and compressive strength of hardened mortar. 2007.

Valluzzi, M.R., da Porto, F., Garbin, E., and Panizza, M. 2014. Out-of-plane behavior of infill masonry panels strengthened with composites materials. Materials and Structures 47:2131-2145.

Figure 1. Masonry walls geometry and reinforcement layout adopted in the experimental test: (a) Original masonry sample; (b) GFRCM_01; (c) GFRCM_02; (d) SRG_01.
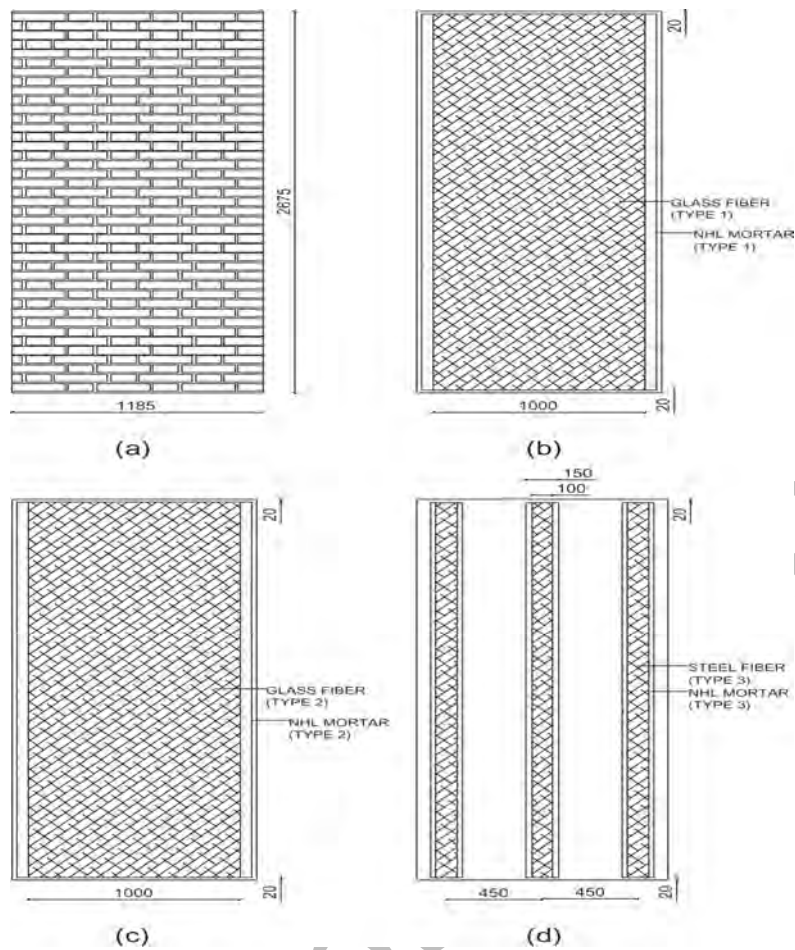
Figure 2. Application of the strengthening systems on the original masonry samples: (a) GFRCM_01; (b) GFRCM_02; (c) SRG_01.

(a) (b) (c)

Figure 3. Phases of the mechanical characterization of masonry materials.

(a)

(b)
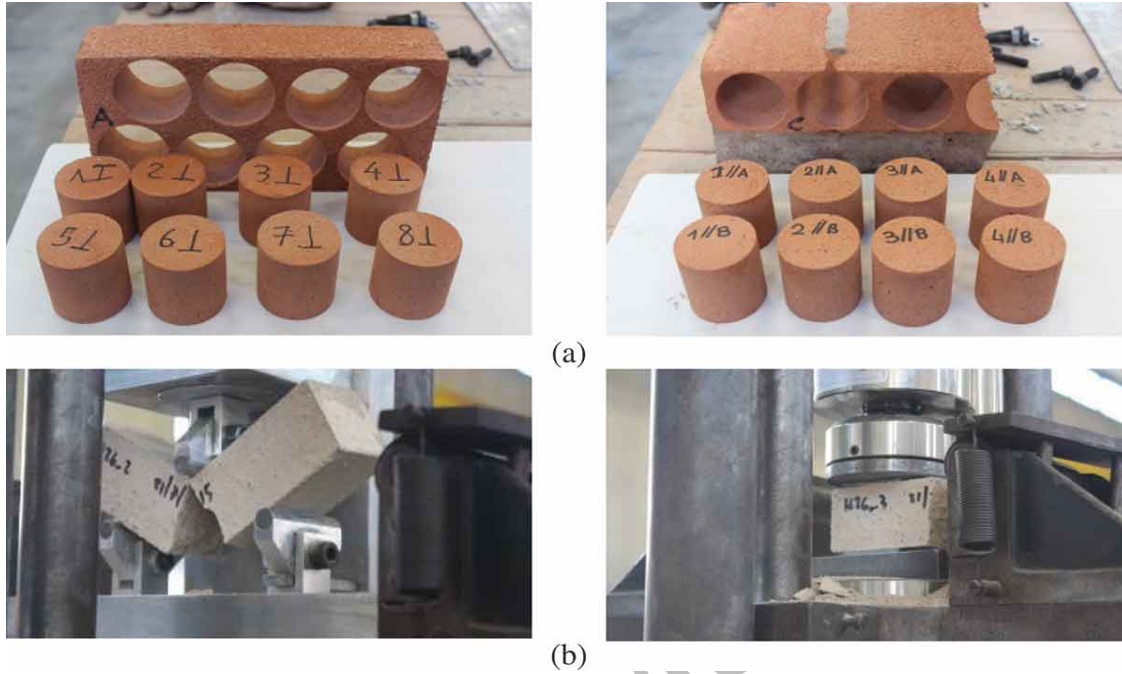
Figure 4. Test set-up designed for the static tests on vertical walls prescribing axial and out-of-plane independent systems of forces.

(a)

(b)
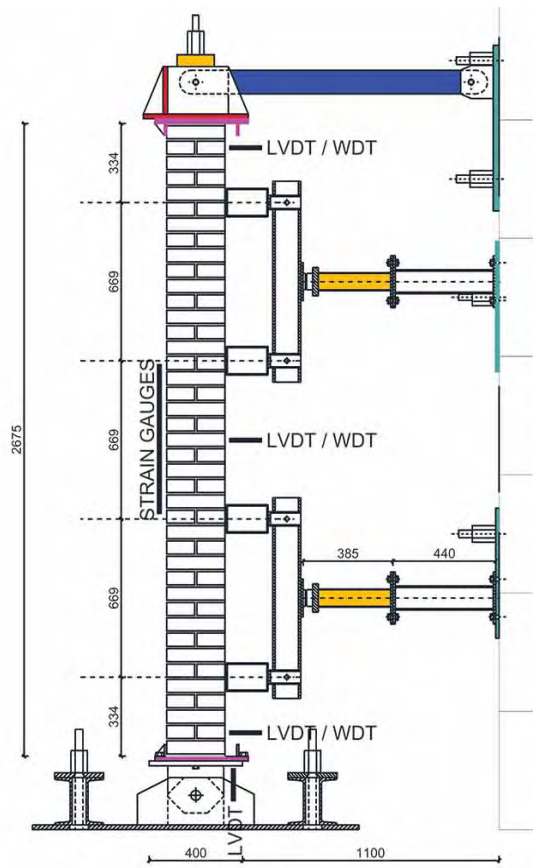
Figure 5. Failure modes of reinforced masonry walls: (a) GFRCM_01; (b) GFRCM_02; (c) SRG_01.

(a)

(b)

(c)

Figure 6. Particular of the cracking scenario on mortar joints at the end of the test on GFRCM_01 wall.
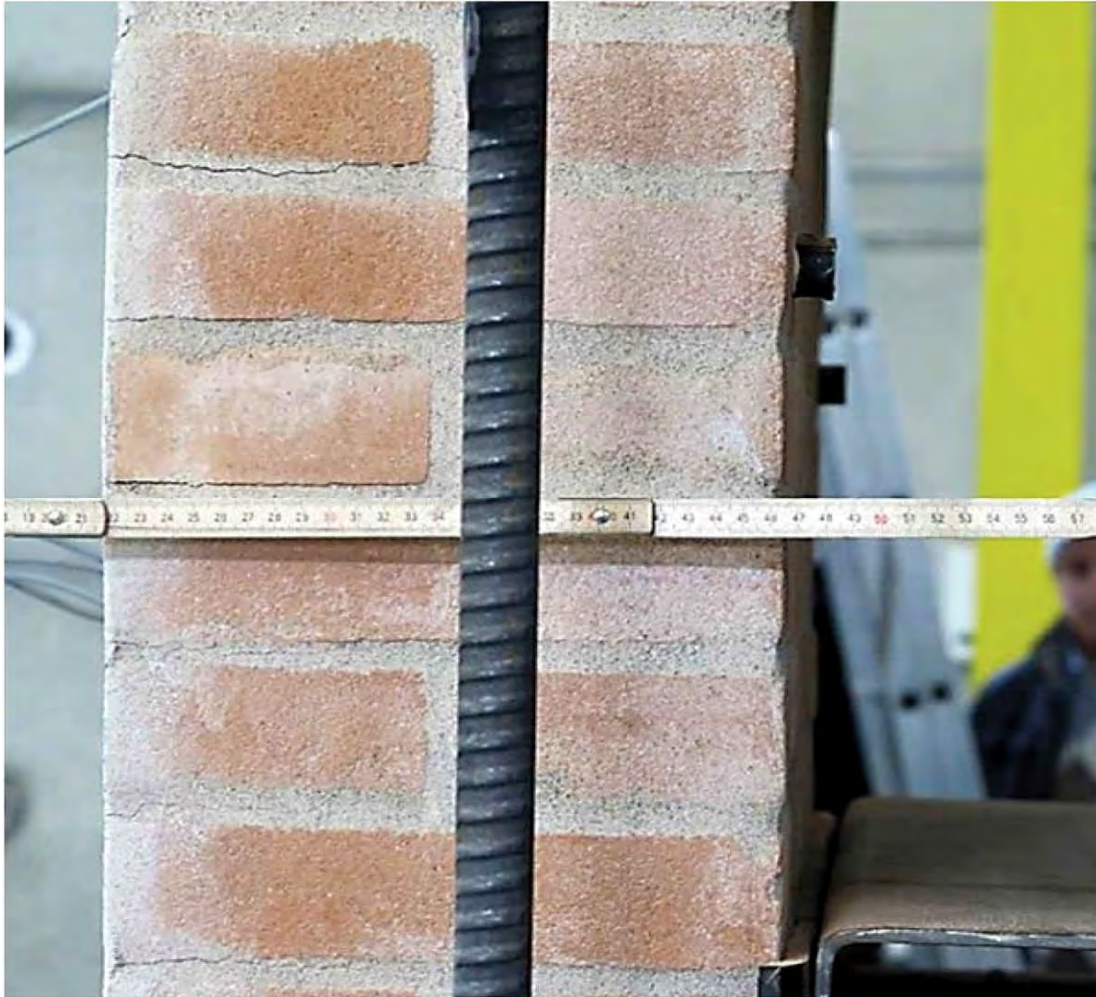
Figure 7. Moment-deflection curve of masonry walls for the mid-height section of the walls and comparison with numerical outcomes: (a) GFRCM_01; (b) GFRCM_02; (c) SRG_01.

(a)

(b)

(c)

38
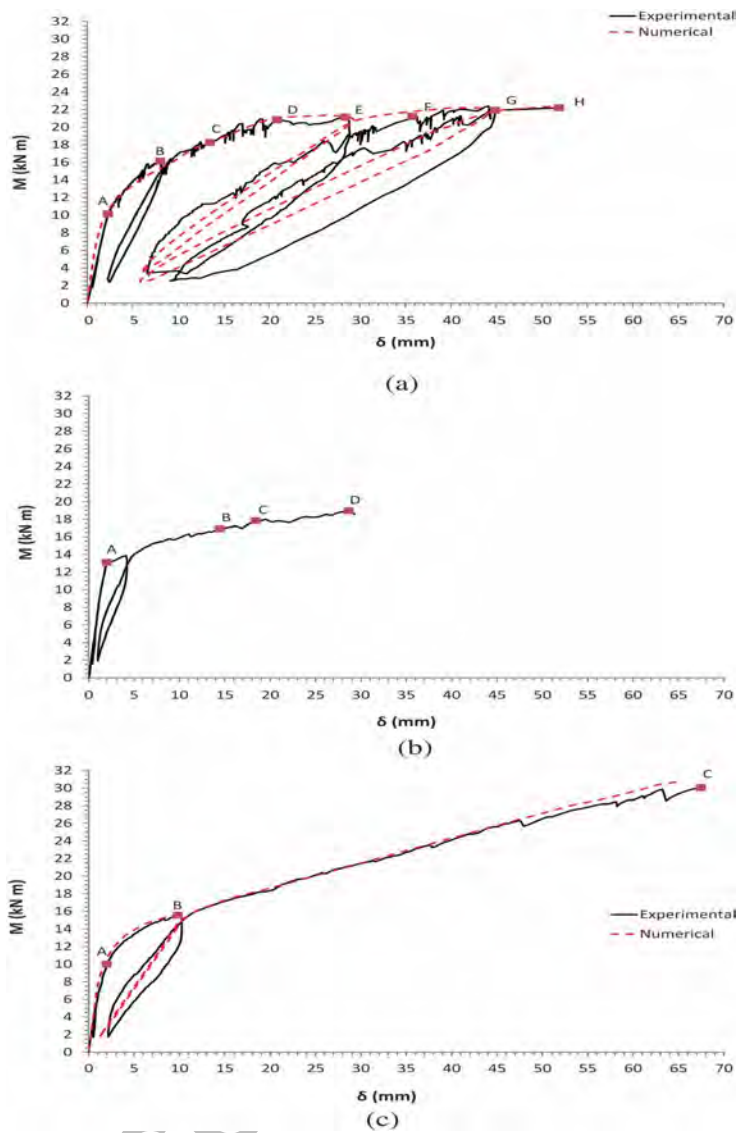
Figure 8. GFRCM_01: bending deflection curves for the load levels identified in Fig.7a and comparison with numerical model.
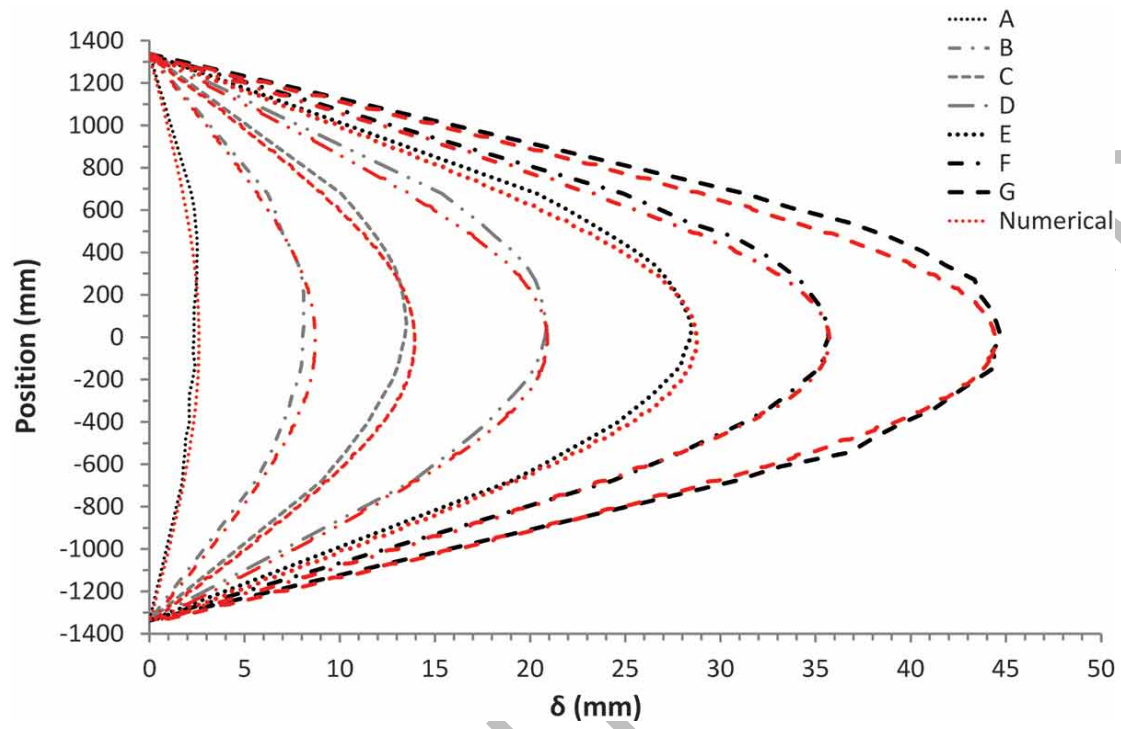
Figure 9. GFRCM_01: evolution of strain field during the test for some of the load levels identified in Fig. 7a: (a) Point C; (b) Point E; (c) Point G.
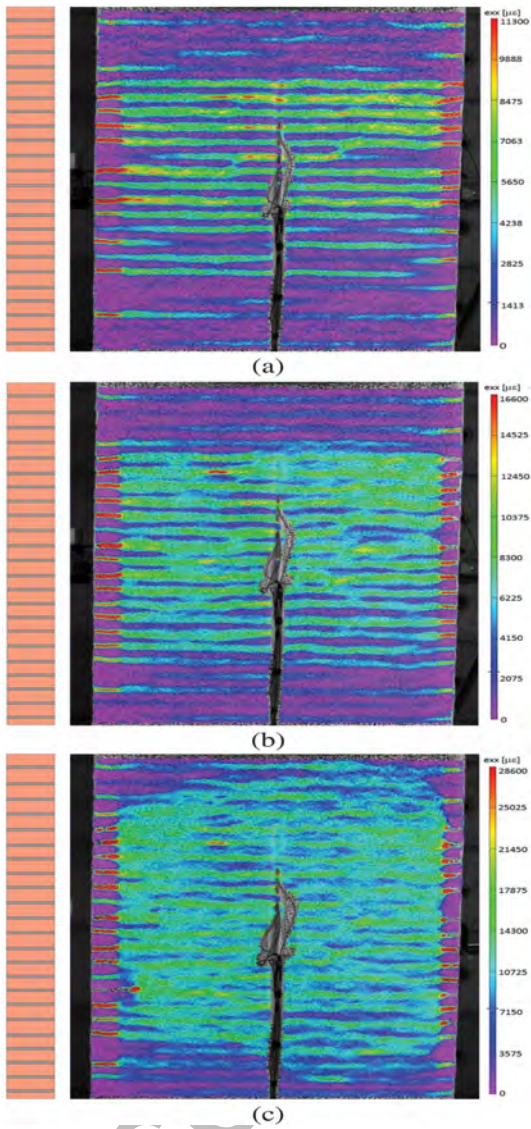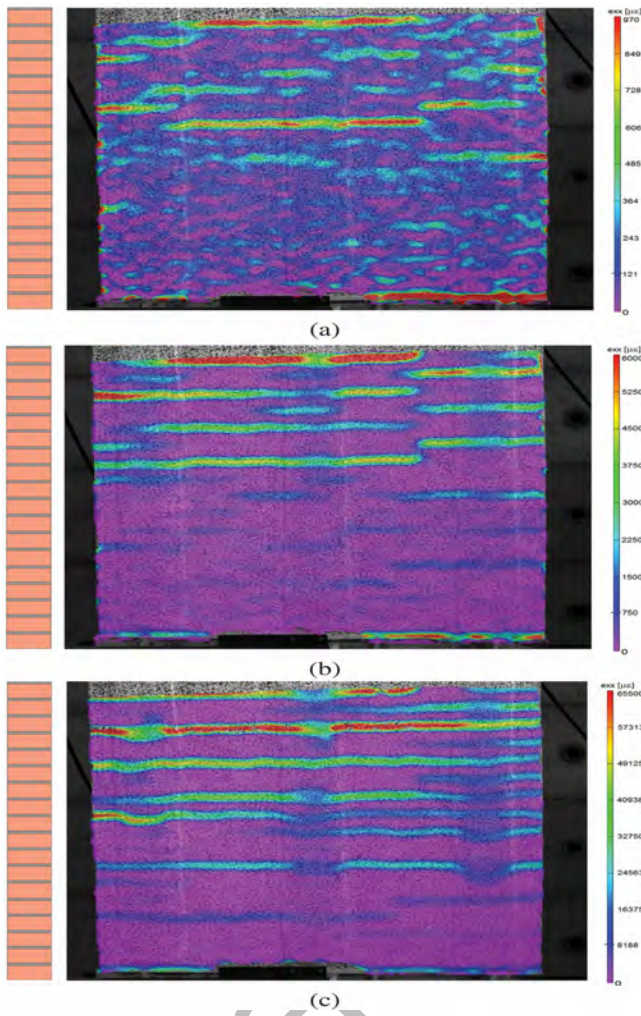
Figure 10. SRG_01: evolution of strain field during the test for some of the load levels identified in Fig. 7c: (a) Point A; (b) Point B; (c) Point C.

Figure 11. Strain redistribution due to the presence of reinforcement: (a) Lines of analysis; (b) Comparison between strain measured on masonry and on the strengthening system surface.
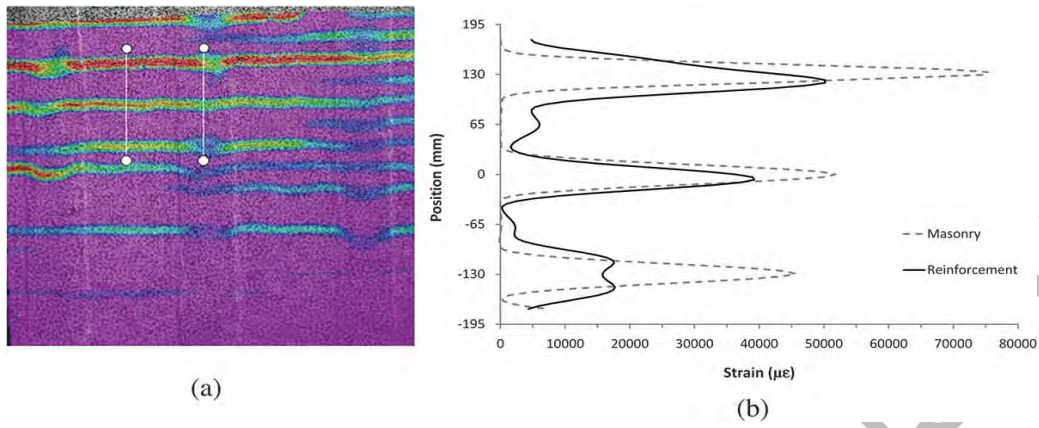

(a)

(b)

Figure 12. GFRCM_02: evolution of strain field during the test for the load levels identified in Fig. 7b: (a) Point A; (b) Point B; (c) Point C; (d) Point D.
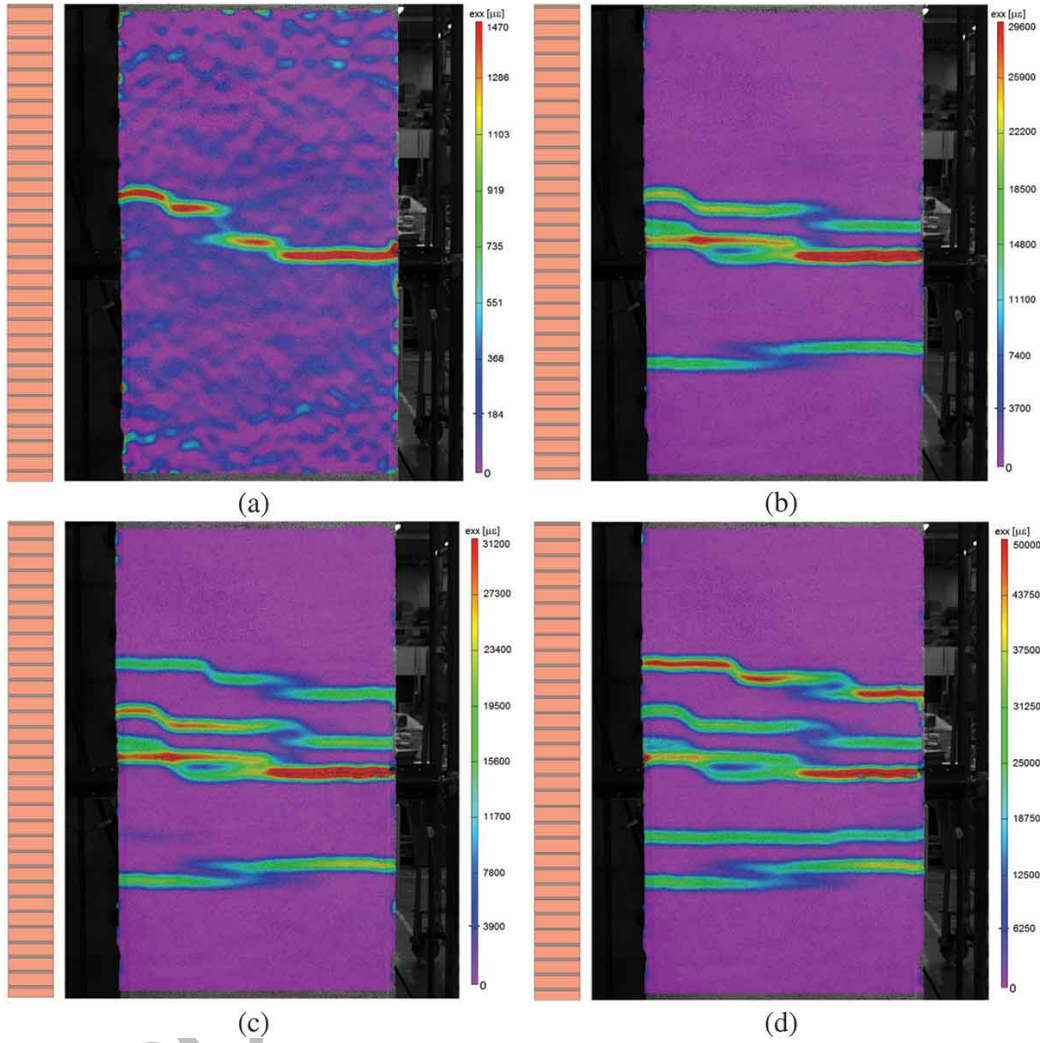
Figure 13. Comparison between strain gauges and DIC technique for some load levels specified in Fig. 7a (GFRCM_01): (a) Strain profiles for point B; (b) Point C; (c) Point G.
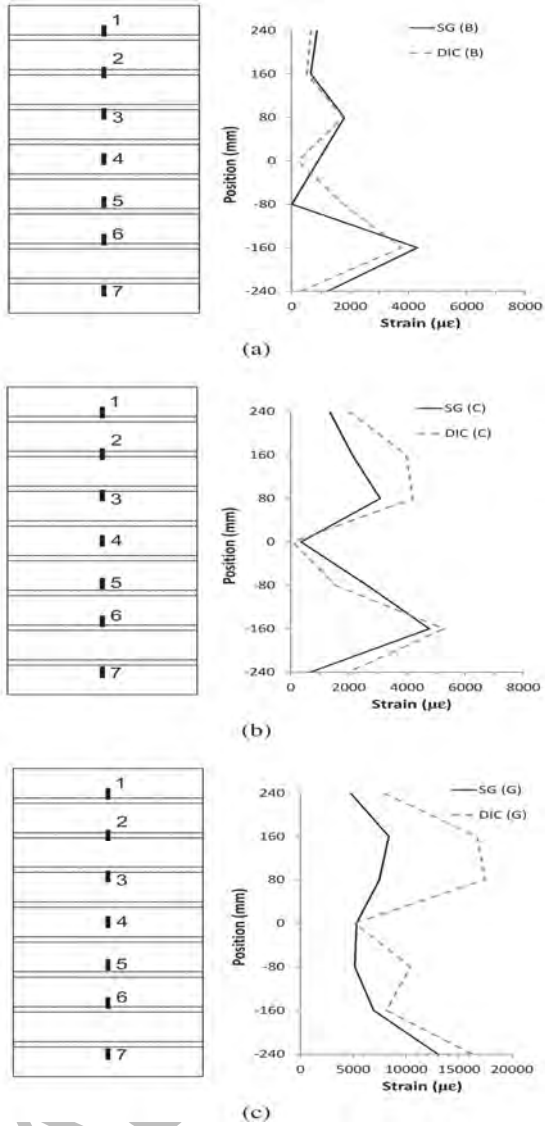

(a)

(b)

(c)

Figure 14. Finite element model adopted for the numerical simulation of the out-of-plane behaviour of the walls: (a) Geometry and texture of the masonry considered for the typical transversal section; (b) Mesh adopted in the analysis with identification of the restraints and the horizontal system of load; (c) Particular of the mesh with specification of the three layers modelling the FRCM reinforcement.
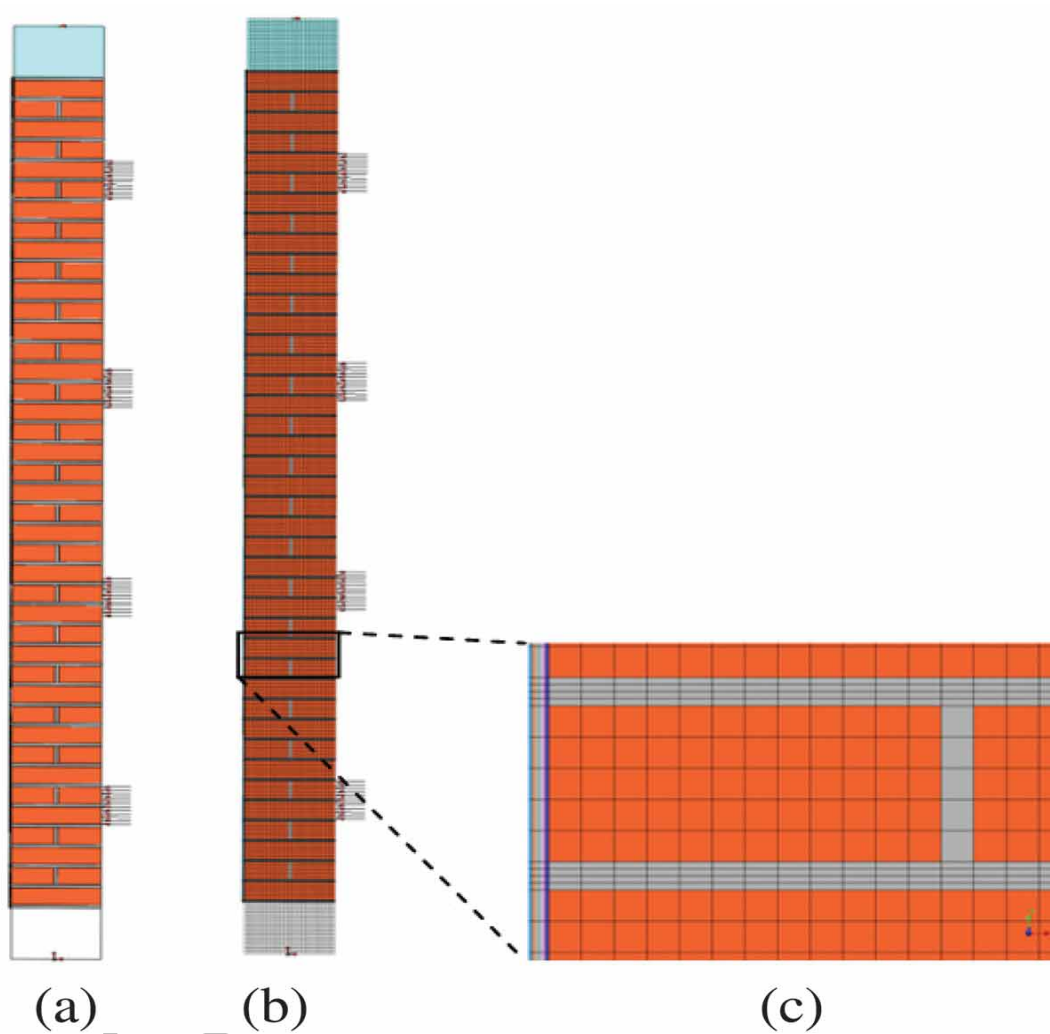

(a)　　(b)　　(c)

Figure 15. Evolution of the crack pattern from the numerical analysis for the specimen GFRCM_01 for the load levels identified in Fig.7a as point A, B, C, D, E and H.
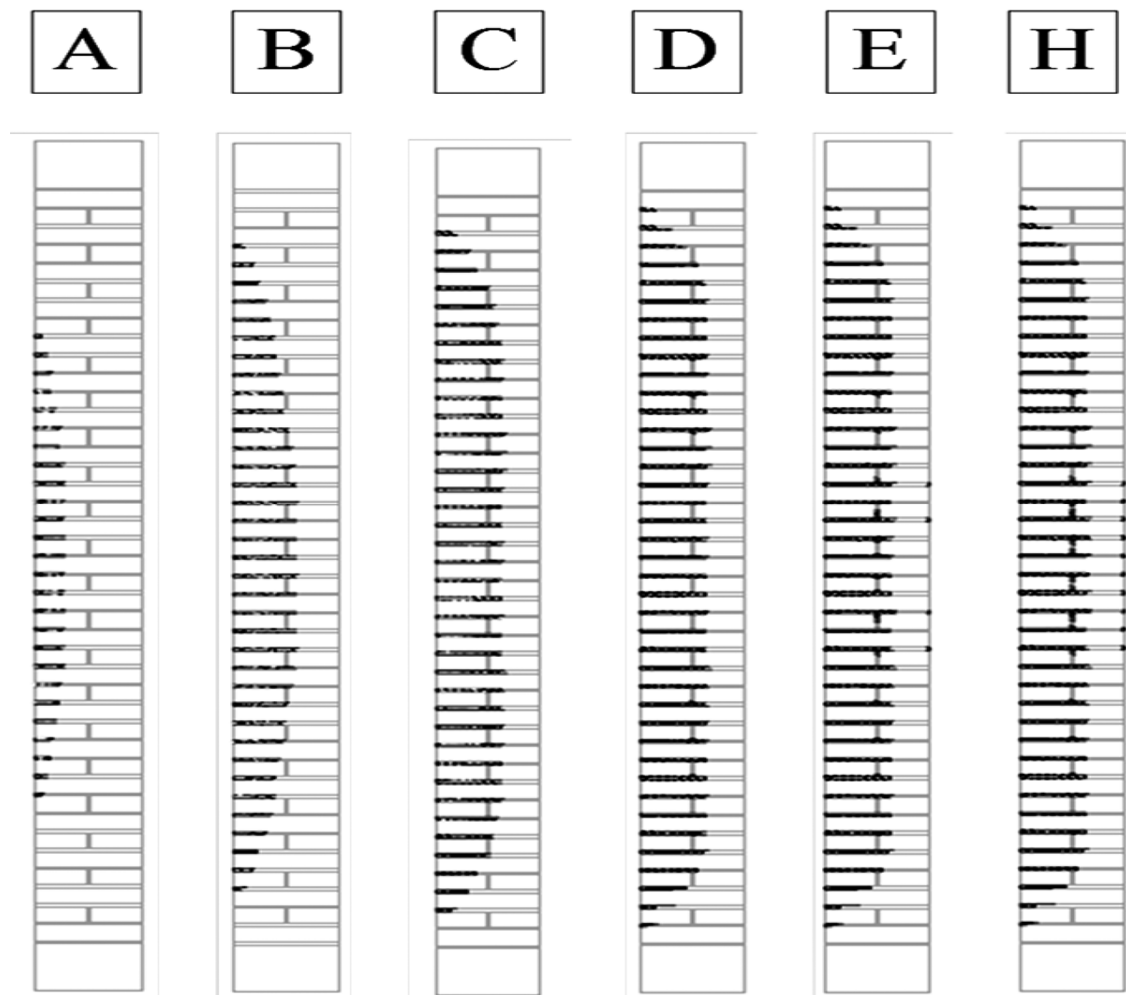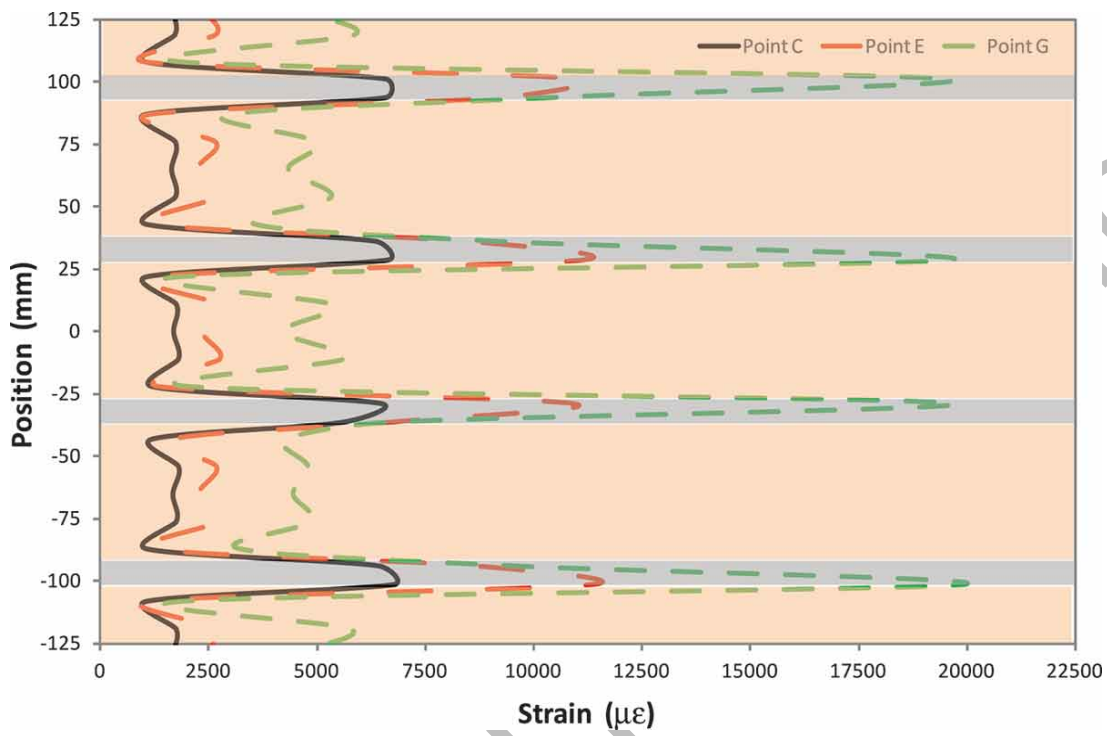
Figure 16. Evolution of strain field obtained from the numerical analysis for the specimen GFRCM_01 for the load levels identified in Fig.7a as point C, E and G.

Table 1. Reinforcement layout.

Sample code	Reinforcement Type	Matrix Type	Adhesion Promoter Type
GFRCM_01	Glass Fiber Grid	Lime-based mortar	IPN
GFRCM_02	Glass Fiber Grid	Lime-based mortar	-
SRG_01	Steel Fiber Sheet	Lime-based mortar	-

Table 2. Brick properties.

Cored direction	f_{bc} (MPa)	$f_{bt,flex}$ (MPa)	$f_{bt,split}$ (MPa)
⊥ to bed	18.64	4.55	2.65
// to bed	22.07	4.75	3.04

Table 3. Mortar properties.

Type of mortar (use)	f_{mc} (MPa)	f_{mt} (MPa)
NHL (Masonry)	0.99	0.34
NHL (GFRCM_01)	10.57	3.72
NHL (GFRCM_02)	13.09	3.25
NHL (SRG_01)	15.25	4.25

Table 4. Prediction of maximum bending moments in relation to the different failure modes and comparison with experimental results.

Sample	$M_{max,URM}$ (kN m)	$M_{max,deb}$ (kN m)	$M_{max,del}$ (kN m)	$M_{max,bond\ tests}$ (kN m)	$M_{max,fiber\ rupture}$ (kN m)	$M_{max,exp}$ (kN m)
GFRCM_01	-	22.80	21.84	18.50	23.31	**22.38**
GFRCM_02	-	22.50	21.76	16.10	18.49	**18.97**
SRG_01	-	18.99	19.09	18.85	25.79	**30.07**
URM wall	8	-	-	-	-	**-**